Indian Journal of Chemistry
Vol. 64, October 2025, pp. 953-961
DOI: 10.56042/ijc.v64i10.20819

Structural and thermal insights into one-step synthesized phosphate-based Mn–pyrazole–oxyhydroxide nanocomposites

Sushree Priyadarshini[a], Gouri Sankhar Brahma[b] & Suprava Nayak*[a]

[a] School of Chemistry, Gangadhar Meher University, Sambalpur 768 004, Odisha, India
[b] Faculty of Science and Technology (IcfaiTech), The ICFAI Foundation for Higher Education, Hyderabad 501 203, Telangana, India
E-mail: suprava7107@gmail.com

Received 19 June 2025; accepted (revised) 25 September 2025

With the industrial sector accounting for 42% of India's total electricity consumption, there is a pressing need to develop energy-responsive materials that can enhance furnace efficiency and reduce overall energy usage. The present study reports the synthesis of a novel Mn–pyrazole–oxyhydroxide nanocomposite designed to combine the redox activity and thermal stability of manganese, the strong coordination ability and heat resistance of pyrazole, and the high thermal conductivity of manganese oxyhydroxide. The composite has been synthesized *via* a simple one-step precipitation method. Following the precipitation, the resulting material is filtered and subjected to two different drying conditions: one at an elevated temperature of 80–90°C, referred to as the calcined material (**SS-1**), with the composition $[Mn_2(\mu\text{-}C_3H_4N_2)(OH)_4(\mu\text{-}HPO_4)_2\cdot(NaHPO_4)_2]\cdot(Mn\text{-}O\text{-}OH)\cdot 2H_2O$; and the other at room temperature, referred to as the non-calcined material (**SS-2**), with the composition $Mn(C_3H_4N_2)(HPO_4)(OH)_4\cdot(MnHPO_4)\cdot(Mn\text{-}O\text{-}OH)_2\cdot(NaH_2PO_4)_2\cdot 2.5H_2O$. Their compositions have been confirmed through ICP-OES, CHNS, and TGA analyses. Powder X-ray diffraction (PXRD) has been performed to determine the crystallite sizes, revealing an average of 83.5 nm for SS-1 and a comparatively smaller size of 60.8 nm for SS-2. FTIR and TGA analyses verified the presence of various atomic binding modes and distinct molecular components, while UV-Vis-NIR spectroscopy provide insights into their band gaps and refractive indices. SS-1 exhibits a band gap of 1.46 eV with a refractive index of 2.84, whereas SS-2 shows a lower band gap of 0.50 eV and a higher refractive index of 3.71. Importantly, DSC analysis reveals low specific heat capacities for both composites, 0.148 J/g·K for SS-1 and 0.167 J/g·K for SS-2. These low specific heat values classify them as low thermal inertia materials. Consequently, both SS-1 and SS-2 demonstrate strong potential as energy-responsive thermal coatings.

Keywords: Manganese-Pyrazole, Manganese-oxyhydroxide, Nanocomposites, Low thermal inertia material

The industrial sector holds the largest share of electricity consumption in India, accounting for 42% of total energy demand. In industrial furnaces, a substantial portion of fuel or electrical energy is expended during the pre-heating phase, making it a key area for energy efficiency improvements. Research efforts have primarily concentrated on minimizing convective heat losses to enhance furnace heating efficiency[1-5]. However, the impact of material properties, particularly specific heat capacity, has received relatively less attention. Incorporating materials with lower specific heat capacity into refractory compositions can enable furnaces to reach target temperatures more rapidly, thereby reducing overall energy consumption. This approach offers a promising avenue for improving energy efficiency in industrial heating systems, supporting sustainable and cost-effective thermal management. Phosphate was chosen as one of the components in this study due to its well documented role as a binder in refractory materials, significantly enhancing thermal stability, chemical resistance, and mechanical strength[6,7]. Furthermore, numerous studies have demonstrated the crucial role of manganese-oxyhydroxide compounds[8,9], manganese-pyrazole-based MOFs[10-12], and manganese-phosphate-based compounds[13] in energy storage technologies. These materials have been extensively utilized as functional additives in electrochemical energy storage systems, electrochemical devices, solar cells, and thermal management coatings. In addition to these properties, elemental manganese has a lower specific heat capacity than aluminum, a metal commonly used in furnace applications. This means that aluminum requires nearly twice the amount of energy to raise the temperature of a unit mass by one degree Kelvin compared to manganese. Considering these advantageous characteristics, a cost-effective inorganic-organic composite incorporating manganese, phosphates, and

pyrazole has been synthesized using a one-step wet chemical method. This study was undertaken as part of our ongoing interest in investigating the thermal behaviour of various phosphate-based materials[14,15]. In the present work, one calcined (SS-1) and another non-calcined (SS-2) nano-composite material have been synthesized and characterized, which have not been reported earlier. The novel materials SS-1 and SS-2 comprising of Mn-Pyrazole and Mn-Oxyhydroxide (Mn-O-OH) with phosphate groups exhibit low specific heat and high refractive index value, enabling rapid heating and cooling. It may be used as additives to enhance the energy efficiency of the furnace or other heating appliances.

Experimental Section

Materials

Analar grade chemicals by Sigma-Aldrich were used for synthesis purpose *viz*. $Mn(CH_3COO)_2.4H_2O$, H_3PO_4, NaOH. Freshly prepared double-distilled solution water was used for solution preparation. All glass distillation system with alkaline $KMnO_4$ was used for the second distillation.

Synthesis

Manganese(II) acetate tetrahydrate (25 mmol) was dissolved in distilled water, and a 25 mmol solution of dilute phosphoric acid was gradually added to the manganese solution with continuous stirring. Stirring was maintained for 1 hour at 273 K to ensure homogenization. Subsequently, an aqueous solution of pyrazole (0.1 mol) was introduced, followed by the addition of freshly prepared NaOH solution to adjust the *p*H to 8.5. The neutralized solution was left stirring for 24 hours. The resulting pinkish white colour precipitate was thoroughly washed with double-distilled water. Half of the obtained precipitate was dried at RT in a desiccator over silica gel, forming a sample referred to as SS-2. The remaining portion was subjected to calcination at 353 K for 6 hours, yielding a sample designated as SS-1.

Instrumentation

The functional groups of both mixtures were identified from the FT-IR spectrum using a Thermo-Nicolet Nexus 670 setup in between 400 to 4000 cm^{-1}. X-ray diffraction (XRD) analysis was carried out on PANalytical Empyrean XRD with Copper Kα radiation (λ=1.5406 Å) having 2θ range of 5 to 80◦, a step of 0.01◦and an acquirement time of 1 s for each step. The crystallite size was determined from FWHM (full width at half maximum) of their XRD peaks) using Debye-Scherrer equation. The iCAP 6500 DUO (Thermo Scientific) inductively coupled plasma-Optical Emission Spectrophotometer (ICP-OES) was used to identify the elements such as Mn, P and Na. The Thermo Scientific Flash EA 1112 (elemental analyzer) was used for C-H-N analysis. The band gap (Eg) of both the mixtures was determined with the help of UV-Vis-NIR analysis (Varian Cary 5000 spectrophotometer). With a heating rate of 10 K/min, the specific heat capacity of the synthesized compound was determined using differential scanning calorimetry (DSC Discovery 250 equipment). All DSC measurements were carried out in the aluminium crucible between the temperature range of 30 to 600°C in a normal atmosphere. Thermogravimetric analysis (TGA), Derivative thermogravimetry (DTG), and Thermal decomposition studies were done in the temperature range of 40 to 600°C on a TAQ600 thermal analyzer in a normal atmosphere using an aluminium crucible. All Characterization of SS-1 and SS-2 were done at STIC-Cochin.

Results and Discussion

Elemental analysis

Elemental analysis of SS-1 and SS-2 was conducted using ICP-OES and a CHN elemental analyzer. For **SS-1**, the synthesized material was found to have the molecular formula $Mn_3C_3H_{17}N_2P_4Na_2O_{24}$ which was interpreted to consist of following composition: $[Mn_2(\mu\text{-}C_3H_4N_2)(OH)_4(\mu\text{-}HPO_4)_2\cdot(NaHPO_4)_2].(Mn\text{-}O\text{-}OH)\cdot 2H_2O$, with a molecular weight of 800.0 g. The calculated elemental composition (%) is Mn (20.61), C (4.50), H (2.14), N (3.50), Na (5.75),P (15.49). The experimentally found values: Mn (20.79), C (3.73), H (2.711), N (4.13), Na (5.79),P (14.44). similar bridged manganese phosphate compounds are reported by Sharma et.al.[16].

For **SS-2**, the synthesized material was assigned with the molecular formula $Mn_4C_3H_{21}N_2P_4Na_2O_{28.5}$ which was proposed to consist of following components in it $Mn(C_3H_4N_2)(HPO_4)(OH)_4.(MnHPO_4)\cdot(Mn\text{-}O\text{-}OH)_2\cdot(NaH_2PO_4)_2.2.5H_2O$ with a molecular weight of 898.8 g. The calculated elemental composition (%) is Mn (24.23), C (3.97), H (2.33), N (3.09), Na (5.07),P (13.66), which closely matches the experimentally determined values: Mn (23.49), C (2.06), H (2.932), N (3.79), Na (4.07), and P (13.90). Furthermore, the above compositions have been

validated through thermogravimetric analysis (TGA), confirming the molecular and compositional integrity of SS-1 and SS-2.

Structural analysis

FTIR

The structural properties of SS-1, which contains a bridged N,N'-coordinated bidentate pyrazole and two bridged hydrogen phosphate groups, and SS-2, which lacks bridged ligands, were investigated using FT-IR spectroscopy (see Fig. 1a, Fig. 1b). The very weak N-H stretching band at 3386 cm^{-1} in SS-1 compared to moderate band at 3328 cm^{-1} in SS-2 suggests deprotonation and coordination of both nitrogen atoms to the Mn centre[17,18]. In both compounds, vibrational bands in the range of 1050–950 cm^{-1} corresponds to the asymmetric and symmetric stretching of O-P-O bonds in PO_4^{3-} (Ref. 19-23). SS-2, which contains only monodentate phosphate groups, exhibits a single strong band around 1018 cm^{-1}, in contrast, SS-1, which contains both bridged bidentate and monodentate phosphate groups, shows band splitting in this region. The broad band around 3400 cm^{-1} is attributed to O-H stretching from water molecules and phosphate groups. This band appears more pronounced in SS-2 due to room-temperature drying, which retains more O-H bonds and enhances hydrogen bonding between components, whereas calcined material SS-1 exhibits a weaker broad band as rapid drying at higher temperatures reduces hydrogen bonding. Additionally sharp peaks around 578 cm^{-1} in both the spectrum are attributed to the vibrations of the Mn–O bonds in MnOOH[24]. Variations in peak positions and intensities between SS-1 and SS-2 suggest differences in crystallinity and hydration, influenced by their distinct drying conditions.

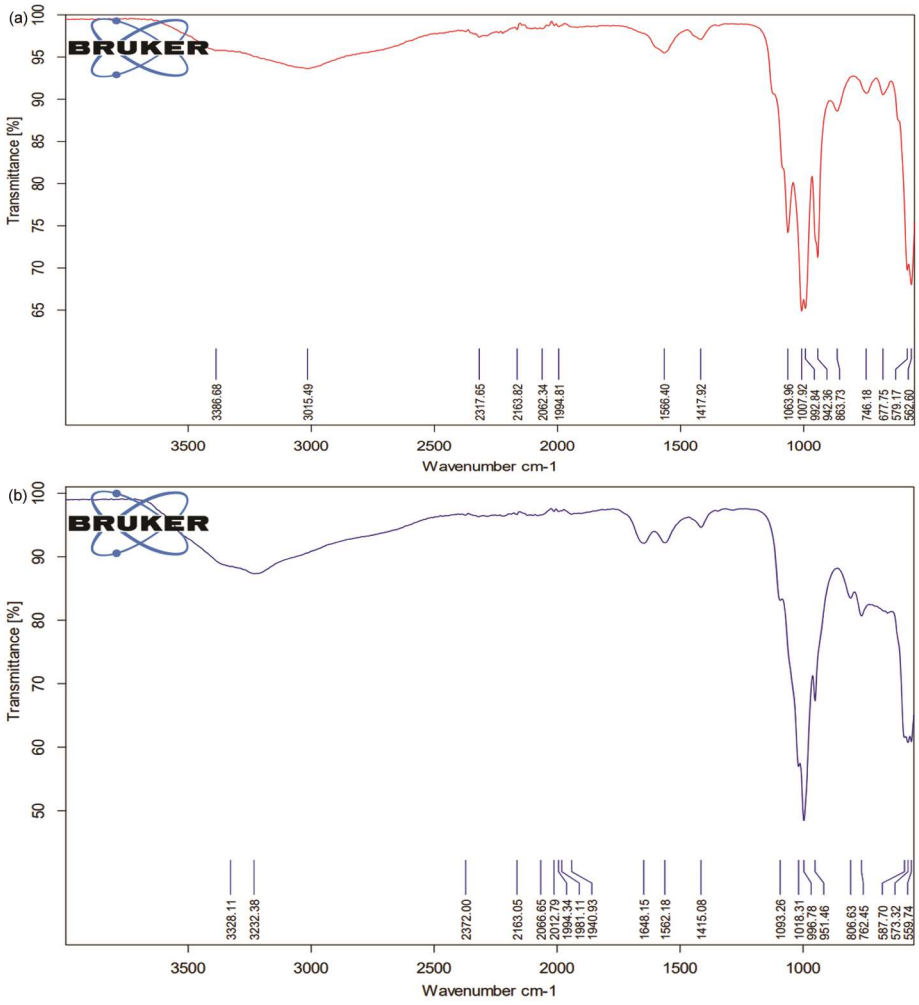

Fig. 1a — FTIR spectrum of SS-1, 1(b); FTIR spectrum of SS-2

X-Ray Diffraction

Fig. 2a presents the X-ray diffraction (XRD) pattern of SS-1, with the crystallite size estimated using the Debye-Scherrer equation based on the full width at half maximum (FWHM) of the most intense peak, yielding a size of 82.3 nm. Additionally, the Williamson-Hall method was used, as shown in Fig. 2b, resulting in a crystallite size of 83.5 nm. Similarly, the XRD pattern of SS-2, shown in Fig. 2c, was analysed using the Debye-Scherrer equation, giving a crystallite size of 59.3 nm, while the Williamson-Hall method, illustrated in Fig. 2d, yielded a value of 60.8 nm[25-27]. Crystallite size determined by Debye-Scherrer equation is slightly less than that calculated by Williamson-Hall method, but these data demonstrate a close agreement between both methods and confirming the reliability of the results. Here SS-1 was found to have a larger crystallite size than SS-2, likely due to variations in drying conditions, where differences in drying temperature influenced the rate of the process. The rapid drying in SS-1 may have led to agglomeration, promoting the formation of larger crystallites compared to SS-2. This suggests that drying conditions play a crucial role in controlling crystallite size. The XRD spectrum provides valuable structural insights into the molecule. A low-angle intense X-ray diffraction peak observed at approximately 8.151° in SS-2 and 11.061° in SS-1 suggests the presence of layered materials or structures with substantial interlayer spacing[28,29], which can be beneficial for thermal management coatings[29]. Additionally, the peak at 26° in both spectra signifies the presence of the Mn-O-OH molecule in these materials [23,30].

Morphology

The SEM images of SS-1 and SS-2 (Fig. 3a and Fig. 3b) reveal a combination of sheet-like structures and flower-like aggregated clusters, indicative of a complex hierarchical morphology typical of manganese oxyhydroxides and phosphates synthesized *via* precipitation methods. Such multi-scale morphologies are advantageous for coating applications, as the sheet structures promote heat spreading and film formation, while the aggregated clusters enhance surface roughness and interfacial bonding. This synergistic architecture supports efficient thermal response, making these materials promising candidates for use as thermally active coatings or additives in industrial applications[31-35]. The high surface area and porous architecture in such material's structures demonstrate how hierarchical morphologies enhance surface interactions, a key advantage for coating adhesion and functional layering.

UV-Vis-NIR

The UV-Vis-NIR spectra were obtained for both materials, and Fig. 4 shows the spectrum of SS-2. The calculated band gap and refractive index of SS-2 were

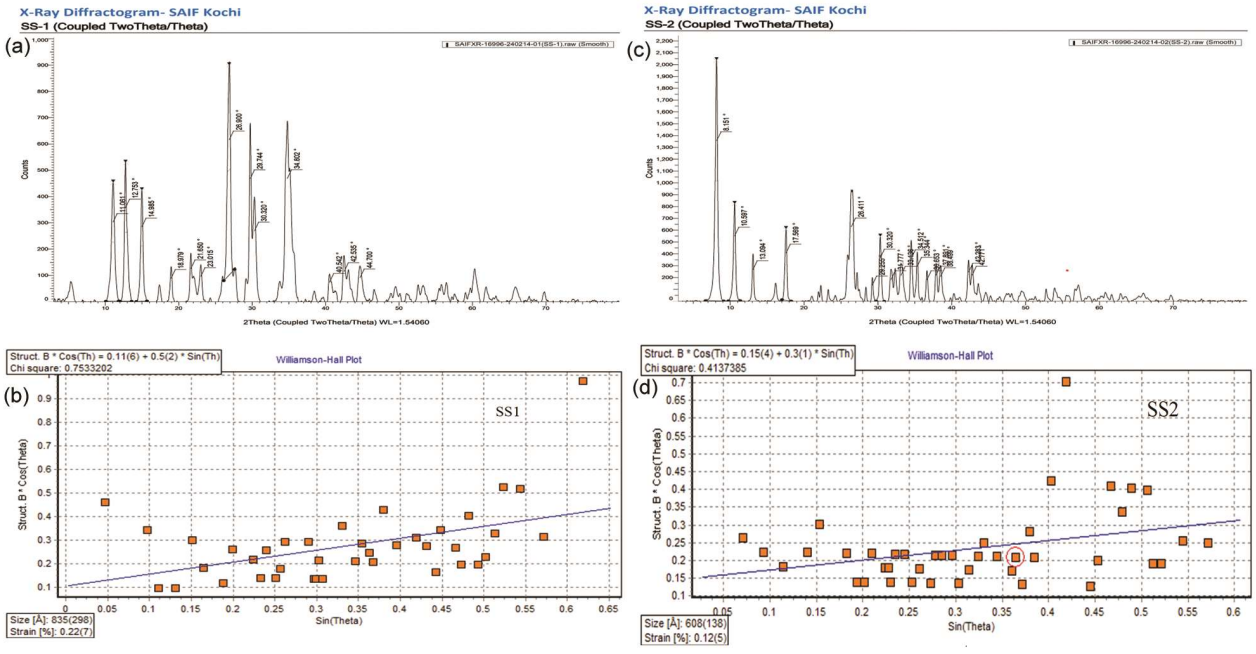

Fig. 2a — XRD Pattern of SS-1, (b); Williamson-Hall plot of SS-1, (c); XRD Pattern of SS-2, (d); Williamson-Hall plot of SS-2.

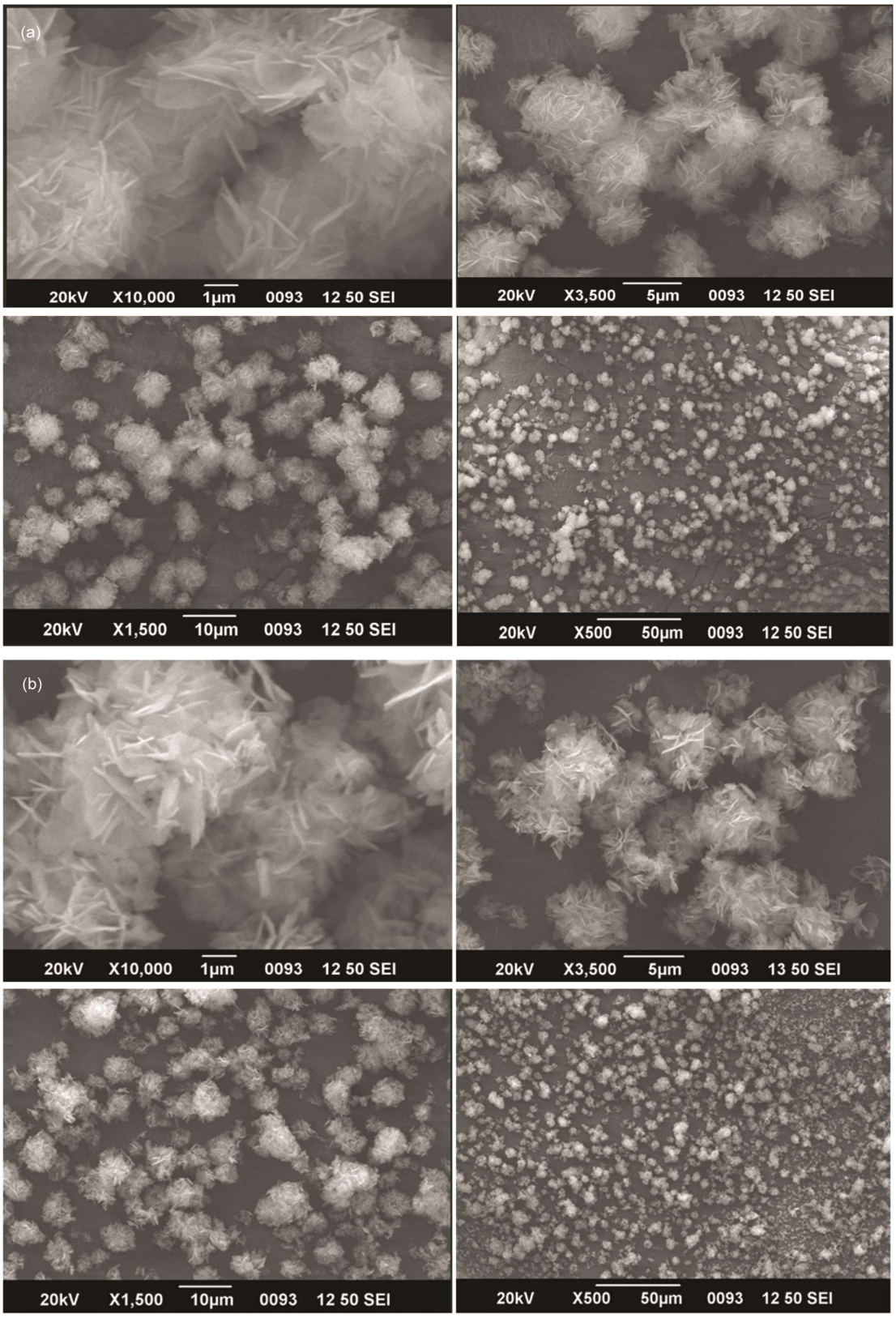

Fig. 3a — SEM Images of SS-1 in different magnifications, (b); SEM Images of SS-2 in different magnifications.

determined to be 0.50 eV and 3.71, respectively, indicating a notably high refractive index[36,37]. Using the absorbance values in Planck's equation, the band gap energy for MnO nanoparticles was estimated to be 3.49 eV. Likewise, UV-Vis-NIR analysis reveals that SS-1 has a band gap of 1.46 eV and a high refractive index of 2.84, determined using the Moss equation[38].

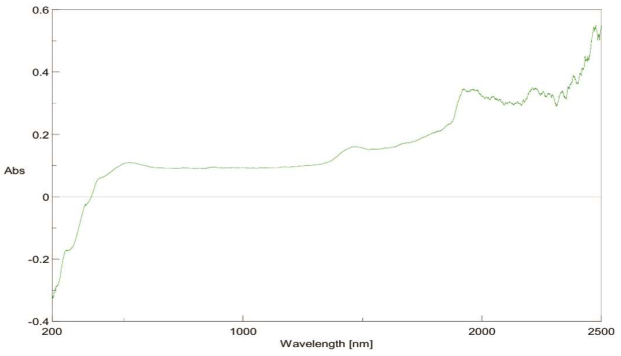

Fig. 4 — Uv-Vis-NIR Spectra of SS-2

Thermal analysis

Thermogravimetry Analysis (TGA)

The TGA-DTG profiles of SS-1 and SS-2, presented in Fig. 5a and Fig. 5b, were recorded over a temperature range of 30°C to 600°C. The DTG curve, which clearly depict three weight loss steps for both the materials. For SS-1 (the calcined material), three distinct weight loss stages are observed at approximately 150°C, 220°C, and 330°C (see Fig. 5a). The first stage accounts for a total weight loss of 6.9%, corresponding to the release of 3.5

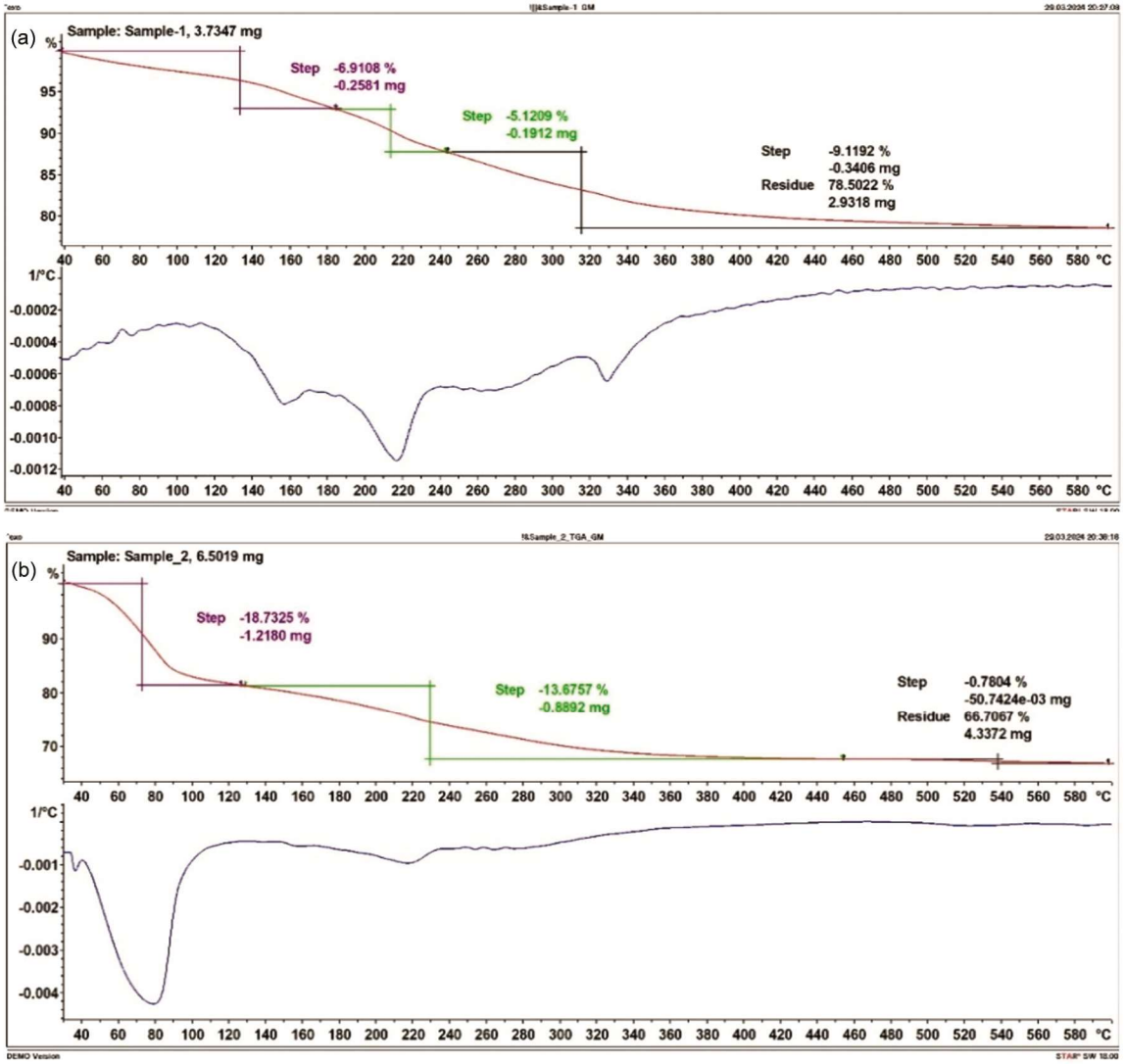

Fig. 5a — TGA-DTG Curve of SS-1, (b); TGA-DTG Curve of SS-2

moles of H_2O—2 moles derived from the water of crystallization, while the remaining 1.5 moles could be removed during the transformation of hydrogen phosphate into phosphate at elevated temperatures [16]. The second weight loss stage is attributed to the elimination of three coordinated hydroxyl (OH) groups, whereas the third stage involves the removal of bridged pyrazole and oxide, leading to a 9.34% mass reduction, which closely matches the experimentally observed value.

In contrast, SS-2 (the non-calcined material) exhibits substantial weight loss at an early stage around 80°C, followed by a moderate second loss at 220°C and a negligible third loss at 280°C (see Fig. 5b). In the first stage, the release of 2.5 moles of water and 1 mole of NaH_2PO_4 leads to a calculated weight loss of 18.35%, which is in close agreement with the experimentally observed 18.7% loss. The second stage involves the removal of an additional NaH_2PO_4 molecule, contributing to a calculated weight loss of 13.57%, which closely matches the experimental value of 13.67%. The third stage shows a minimal loss, likely due to the release of approximately 0.5 moles of water (~1.0%), possibly resulting from the conversion of $MnHPO_4^-$ to $Mn_3(PO_4)_2$[16,39] or the transformation of Mn-O-OH into Mn_2O_3 (Ref. 40). These results validate the predicted compositions of both SS-1 and SS-2. Similar TGA profiles are reported for manganese oxyhydroxide and related compound[40,41]. The residual weight of SS-1 is 78.5%, whereas for SS-2, it is 66.7%. This difference may be attributed to the high-temperature drying of SS-1, which leads to the loss of hydration water. This process could enhance direct interactions between metal ions and ligands, potentially strengthening these bonds. In contrast, the slow drying of SS-2 at RT helps preserve weak hydrogen bonding between its components, resulting in greater weight loss upon heating and a distinct thermal decomposition pattern[42].

Differential Scanning Calorimetry (DSC)

DSC provides critical insights into material behaviour under thermal stress, making it a valuable tool for optimizing materials used for thermal management application. DSC curve of SS-1 is shown in Fig. 6a shows a gradual exothermic trend with a notable peak at 560.74°C. The exothermic peak

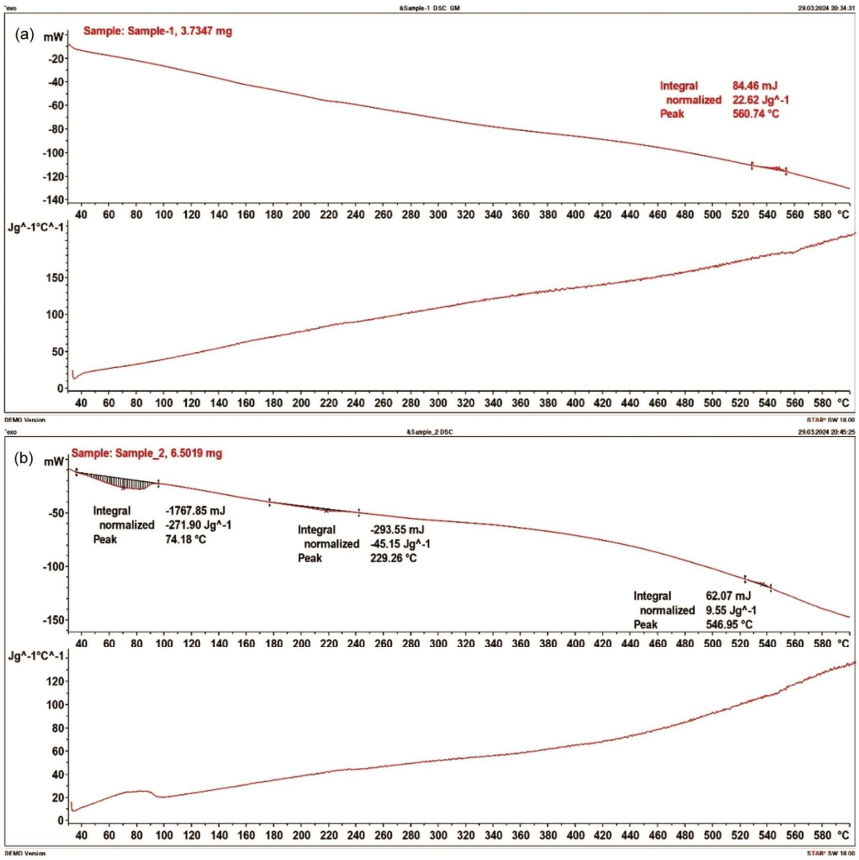

Fig. 6a — DSC Curve of SS-1, (b); DSC Curve of SS-2

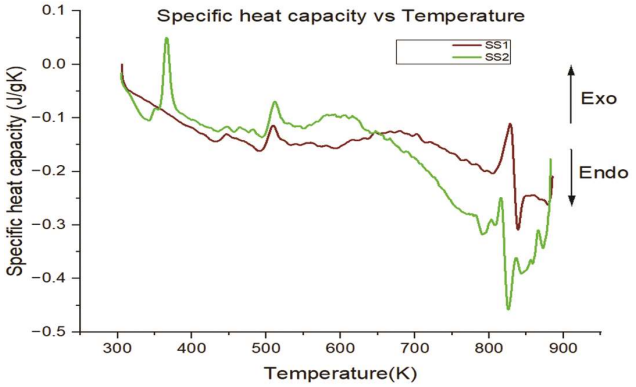

Fig. 7 — Plot of specific heat capacity of SS-1 and SS-2 *versus* temperature.

around 560°C correspond to the third weight loss step in TGA with an enthalpy of 22.62 J/g. The sharp peak suggests a major structural change in the material due to decomposition of residual hydroxyl groups or trapped water. The average specific heat capacity of SS-1 was found to be 0.148 J/g°C.

DSC curve of SS-2 is shown in Fig. 6b. Two endothermic peaks and one exothermic peak were observed from DSC curve. The endothermic peak around 74°C and 229°C correspond to the first and second weight loss step in TGA with an enthalpy of -271.90 J/g and -45.15 J/g respectively. The exothermic peak around 546°C correspond to the third weight loss step in TGA with an enthalpy of 9.55 J/g. The average specific heat capacity of SS-2 was found to be 0.167 J/g°C. The two endothermic peaks and one exothermic peak hints at a phase transition to a more crystalline form, which also reflects its stability at higher temperature. According to the literature, manganese phosphates exhibit excellent thermal stability up to 735°C [35]. Additionally, Song *et al.*[43] reported that the molar heat capacity of Mn-Metal Organic Framework is 341.9 J mol^{-1} K^{-1} at 298.15 K.

The specific heat capacity(Cp) *versus* temperature curve of SS-1 and SS-2 provides a comparative analysis in the Fig. 7. The curve highlights thermal response *i.e.* differences in their thermal stability and energy absorption characteristics over a wide temperature range. SS-1 exhibits a relatively constant Cp than SS-2, which is shows more fluctuation in Cp.

Conclusion

Two materials, SS-1 and SS-2, composed of Manganese, Pyrazole, Phosphate and Mn-Oxyhydroxide with different compositional arrangements, were synthesized using simple precipitation method and thoroughly characterized. SS-1, calcined at 80°C, exhibited lower hydration, stronger Mn-O and Mn-N bonds, larger crystallite size, and greater thermal stability. In contrast, SS-2, dried at RT (non-calcined), retained more water, promoted stronger hydrogen bonding, resulted in smaller crystallites, and displayed altered properties. The study highlights the superior thermal stability of SS-1, making it more suitable for high-temperature applications. These materials, characterized by low specific heat capacity, hence can undergo rapid heating and cooling. Furthermore, the presence of nanosized particles enhances thermal performance through increased surface interactions. Such properties make these materials advantageous for industrial furnace applications, where rapid heating can contribute to energy savings during preheating.

Statements and Declarations

Funding

The authors declare that no funds, grants, or other support were received during the preparation of this manuscript.

Conflict of Interest

The authors have no relevant financial or non-financial interests to disclose.

Author Contributions

All authors contributed to the study conception and design. Material preparation, data collection and analysis were performed by all authors (Sushree Priyadarshini, Gouri Sankhar Brahma and Suprava Nayak). The first draft of the manuscript was written by Sushree Priyadarshini and all authors commented on previous versions of the manuscript. All authors read and approved the final manuscript.

Data availability

The datasets generated during and/or analysed during the current study are available from the corresponding author on reasonable request.

Acknowledgements

Authors SP and SN are thankful to Gangadhar Meher University, Sambalpur, Odisha for giving necessary facilities. GSB is thankful to ICFAI Tech, IFHE, Hyderabad for granting permission to get associated with this work.

References

1 Nandy R N & Jogai R K, *Int J Metall Eng*, 1 (2012) 117.
2 Nezamaddin R, Rahim Z & Abolfazl A, *Recent Adv Petrochem Sci*, 7 (2020) 555710.
3 Souzaa T.M., Luza A P, Santos T J, Gimenesa D C, Migliolia M M, Correab A M & Pandolfellia V C, *Ceramic Int*, 40 (2014) 1503.
4 Meng J, Fang H, Wang H, Wu Y, Wei C, Li S, Geng X, Li X, Zhang J, Wen G & Wang P, *App Ceramic Tech*, 20 (2023) 1350.
5 Dahotre N B, Kadolkar P & Shah S, *Surf Int Anal :Int J Dev App Tech Anal Surf Int Thin Fil,* 31 (2001) 659.
6 Abyzov V A, *Procedia Eng,* 206 (2017) 783.
7 Hopp V, Masoudi A A, Hahn D & Quirmbach P, *Materials* (*Basel*), 14 (2021) 4636.
8 Sathyan T V, Thomas J & Thomas N, *Int J Hyd Energ*, 48 (2023) 38309.
9 Ghodbane O, Pascal J L, Fraisse B & Favier F, *ACS Applied Mat Int*, 2 (2010) 3493.
10 Theerthagiri J., Karuppasamy K., Raj J C, Maia G, Kumari M L A, Kennedy L J, Souza M K R, Cardoso E S F, Kheawhom S, Kim H S & Choi M Y, *Coord Chem Rev*, 513 (2024) 215880.
11 Feng C, Lv C P, Zhao H, Li Z Q, Xie W N, Sun L N & Wang Y, *Cry Growth Design*, 20 (2020) 5682.
12 Smernik J. F., P. Gimeno-Fonquemie. Pol, J. Albalad. Jorge, T. S. Jones, R. J. Young, N. R. Champness, Doonan C J, Evans J D & Sumby C J, *Cryst Eng Comm,* 25 (2023) 6539.
13 Zong J, Peng Q, Yu J & Liu X, *J Power Sour*, 228 (2013) 214.
14 Brahma G S, Sahu A K & Nayak S, *Indian J Chem*, 63 (2024) 797.
15 Samala S, Brahma G S & Swain T, *Monatshefte für Chemie-Chemical Monthly*, 151 (2020) 141.
16 Sharma C V K, Chusuei C C, Clerac R, Moller T, Dunbar K R & Clearfield A, *Inorg Chem*, 42 (2003) 8300.
17 Zerbi G & Alberti C, *Spectrochim Acta*, 18 (1962) 407.
18 Shurvell H F, *Handbook of Vibrational Spectroscopy*, (John Wiley & Sons, Ltd) 2006.
19 Pothiraja R, Sathiyendiran M, Steiner A & Murugavel R, *Inorg Chim Acta*, 372 (2011) 347.
20 Kalita A C, Roch-Marchal C & Murugavel R, *Dalton Trans*, 42 (2013) 9755.
21 Sathiyendiran M & Murugavel R, *Inorg Chem*, 41 (2002) 6404.
22 Murugavel R, Choudhury A, Walawalkar M G, Pothiraja R & Rao C N R, *Chem Rev*, 108 (2008) 3549.
23 Shanmugam S, Ravichandran K, Narayanan T S & Lee M H, *RSC Adv*, 5 (2015) 988.
24 Masoud S-N, Esmaeili-Zare M, Gholami-Daghian M & Bagheri S, *High Temp Mat Proc*, 35 (2016) 493.
25 T Ungár, *Scr Mater*, 51 (2004) 777.
26 Williamson G K & Hall W H, *Acta Met*, 1 (1953) 22.
27 Lucks I, Lamparter P, Xu J & Mittemeijer E J, *Mat Sci Forum*, 443–444 (2004) 119-122.
28 Djamil J, Hansen A-L, Backes C, Bensch W, Schürmann U, Kienle L, Duvel A & Heitjans P, *Nanoscale*, 10 (2018) 21142.
29 Okamoto N L, Hatakeyama T, Li H & Ichitsubo T, *Rigaku J*, 39(2023)1.
30 Xi G, Peng Y, Zhu Y, Xu L, Zhang W, Yu W & Qian Y, *Mat Res Bull*, 39 (2004) 1641.
31 Raju K, Han H, Velusamy D B, Jiang Q, Yang H, Nkosi F P, Palaniyandy N, Makgopa K, Bo Z & Ozoemena K I, *ACS Energy Lett*, 5 (2019) 23.
32 Chun L, Zhong, Chen S S, Dong C, Chen X H & Zhou Q F, *Micro & Nano Lett*, 8 (2013) 325.
33 (**a**) Wang L, Duan G, Chen S-M & Liu X, *J Alloys Comp*, 752 (2018) 123. ;(**b**) Wang W, Jiao T, Zhang Q, Luo X, Hu J, Chen Y, Peng Q, Yan X & Li B, *RSC Adv*, 5(2015) 56279.
34 Sathyan T V, Thomas J & Thomas N, *Int J Hyd Ene*, 48 (2023) 38309.
35 Neher G & Salguero T T, *Cryst Growth Des,* 17 (2017) 4864.
36 Tirukoti M, Belagali S L & Vadiraj K T, *Mat Today: Proc,* 75 (2023) 72.
37 Srivastava G, Dalela S, Gautam N K, Kumar S, Hashmi S Z, Ahmad M A, Quraishi A M, Khanna V & Alvi P A, *Nano Trends*, 9 (2025) 100067.
38 Moss T S, *Physica Status Solidi (b*), 131 (1985) 415.
39 Murugavel R, *Emergent Mat*, 2 (2019) 273.
40 Lee J A, Newnham C E, Stone F S & Tye F L, *J Solid State Chem*, 31 (1980) 81.
41 Ping Z, Song L, Lu H, Hu Y, Xing W, Ni J & Wang J, *Poly Degrad Stab*, 94 (2009) 201.
42 Rafika A H, Khunur M M., Tjahjanto R T & Prananto Y P, *Kuwait J Sci*, 50 (2023) 596.
43 Li-Fang Song, Jiang C-H, Cheng-Li J, Zhang J, Li-Xian S, Xu F, Jiao Q-Z & Xing Y-H, *J Therm Anal Calor*, 102 (2010) 1161.